



GLASS FIBER REINFORCED POLYPROPYLENE NANOCOMPOSITES

**Chrystèle Houphouët-Boigny*, Christopher J.G. Plummer*, Martyn D. Wakeman*,
Véronique Michaud*, Jan-Anders E. Månson***

***Laboratoire de Technologies des Composites et Polymères (LTC), Ecole Polytechnique
Fédérale de Lausanne (EPFL), 1015 Lausanne, Switzerland**

Keywords: *polypropylene, nanocomposites, glass mat thermoplastics, impregnation*

Abstract

Thermoplastic polypropylene-montmorillonite clay nanocomposites have been investigated as an alternative to pure polypropylene as the matrix for glass mat thermoplastic (GMT) composites. The impregnation kinetics and the mechanical properties of the final consolidated composites are discussed in terms of the montmorillonite dispersion and its influence on the rheological and mechanical properties of the nanocomposite precursors. The observed increases in the matrix melt viscosity in the presence of montmorillonite were reflected by increases in impregnation times, consistent with models based on the assumption of Newtonian flow through a porous medium. Impregnation rates are considered compatible with industrial GMT process requirements. The bending stiffness and strength of consolidated GMT specimens was found to increase significantly with montmorillonite content, although the impact strength decreased somewhat.

1 Introduction

The availability of commercial masterbatches for dispersing montmorillonite (MMT) in polypropylene (PP) has driven interest in combining PP nanocomposites with conventional composite technology to form hybrid materials [1]. To be competitive, such materials must show property improvements (heat stability, flame resistance, barrier properties etc.) without significant increases in system cost. Processing is also a potentially important issue in this context, because even low concentrations of MMT (1 to 2 wt%) may cause substantial changes in melt behavior [2]. However, these changes are expected to be less critical for thermoplastic matrices than for thermosets, given that one of the primary goals of thermoplastic

composite processing routes is to facilitate impregnation by reducing the resin flow distances.

The feasibility of two strategies for hybrid composites has been demonstrated previously: (a) commingled glass fiber (GF)/PP-MMT fibers; (b) hybrid glass mat thermoplastics (GMT) from PP-MMT films [3]. GMT composites are semi-finished materials consisting of random glass fiber mats, in chopped or continuous form, impregnated with PP. They are typically prepared from two GF mats interleaved with three PP films using a double belt laminating press at pressures of 2 to 3 bar [4]. Advantages for automotive applications include short processing times, high impact strength, low cost and weight saving. Products are generally manufactured from the semi-finished GMT in a single forming operation. Two basic requirements must be met if the competitiveness of semi-finished composite materials in general and of GMTs in particular is to be maintained. These are: (i) the availability of processing techniques suitable for converting the materials at a competitive cost and in adequate volumes; (ii) adequate impregnation, notably within fiber bundles, during the production of the semi-finished material so as to optimize the quality of parts produced using subsequent rapid forming processes [5]. In what follows, the processing and properties of a hybrid PP-MMT GMT are described, with emphasis on impregnation, the mechanical properties of the precursors and the final consolidated composites. The aim is to assess the potential of this technology for industrial production and the extent to which the MMT influences the properties of the final products.

2 Experimental

GMT grade PP and a PP-MMT concentrate (C.44PA Nanomer® from Nanocor) were

compounded in a 16 × 15 D Prism twin-screw extruder, with the temperatures of the successive zones from the feeder to the die set to 180 °C, 200 °C and 200 °C respectively and a screw speed of 40 rpm, to give a base resin containing 5.9 wt% MMT. Resins with lower MMT concentrations (1 wt%, 2.4 wt%, 3.4 wt% and 5.9 wt% MMT) were prepared by further compounding with PP. PP-MMT films of about 75 mm in width and 0.5 to 0.7 mm in thickness were produced using the same extruder equipped with a Prism TSE calendar system. The extrusion conditions were as for compounding and the calendar temperature was set to 25 °C and the rotation rate to 1 rpm. The GF mat was a 2D needled planar random mat with a nominal fiber length of 50 mm. The fibers were arranged in bundles of typically 100 single fibers and the areal density was 600 g/m².

Impregnation was investigated using a preform consisting of 3 adjacent layers of PP or PP-MMT film placed over 3 layers of the GF mat, giving sufficiently large flow distances for characterization of transient states to be possible with the present experimental set-up. The preform was placed in a pre-heated 50 × 80 mm² shear edge mold for 10 min at 200 °C. A transverse force of 1000 N, corresponding to a pressure of 0.2 MPa, was then applied for different nominal impregnation times, *t* (0 s, 30 s and 10 min), using a hydraulic press (Interlaken), after which the specimens were cooled under pressure by circulating water in the mold walls. These nominal impregnation times did not include the time necessary to close the mold so that a certain amount of infiltration under pressure was expected to take place prior to *t* = 0. The above conditions were chosen to be consistent with the industrial processing, i.e. constant temperature and pressure, absence of transverse flow and a fiber volume fraction of approximately 0.13 [6].

The same procedure was also used for preforms comprising 3 PP or PP-MMT films interleaved with 2 GF mats, a geometry representative of that used in industrial GMT processing. After impregnation, the preforms were consolidated for mechanical testing in a Fontjine hydraulic press using a 50 × 120 mm² closed mold. The specimens were heated to 200 °C for 10 min at a constant pressure of 2 MPa, maintained at 200 °C for another 10 min and then rapidly cooled, giving specimens with less than 2 vol% porosity as determined from optical microscopy, where 50 images per specimen were taken using an Olympus light microscope model BX61 equipped with a

motorized stage. Image analysis was performed using the Analysis software package (Soft Imaging System GmbH).

The state of dispersion and intercalation of the MMT were investigated qualitatively by transmission electron microscopy (TEM, Philips CM-20 operated at 200 kV) and quantitatively by wide-angle X-ray diffraction (WAXS, Siemens Kristalloflex 805 diffractometer at room temperature, Cu K^α radiation, $\lambda = 1.54 \text{ \AA}$). For TEM, samples taken from selected specimens were embedded in epoxy resin, trimmed using a glass knife and stained by immersion in aqueous RuO₄. Ultra-thin sections (50 to 100 nm in thickness) were then prepared at ambient temperature using an ultramicrotome (Reichert-Jung Ultracut-E) equipped with a diamond knife (Diatome). The flow behavior of the PP-MMT nanocomposite resins was investigated by shear rheometry. The resins were compression molded into 0.9 mm thick disks of 25 mm in diameter. Steady-state shear measurements in the cone-plate geometry (0.1 rad) were carried out at 200 °C using an ARES rheometer (Rheometrics Scientific). For glass fiber volume fraction and void content analysis, 10 × 15 mm² sections were cut with a diamond saw from the impregnated glass mats and embedded under vacuum in an Epofix resin (Struers) colored with a fluorescent dye to maximize the contrast between the polymer matrix and the filled voids. Three specimens were analyzed for each set of experimental conditions.

Three-point flexural tests were carried out on 25 × 50 mm² specimens machined from the consolidated plaques at room temperature, 50 °C and 90 °C, using a screw driven UTS tensile testing machine (Test System GmbH). Six tests were made for each specimen type. The span length was 32 mm and the crosshead displacement speed was 2 mm min⁻¹, following the ASTM 790 standard. 70 × 70 mm² specimens taken from the consolidated plaques were also subjected to instrumented falling weight impact (IFWI) tests at room temperature and 90 °C using a Rosand IFW 8 (the specimens were heated to 90 °C in an oven for 15 min and then immediately tested in air). The clamped diameter was 40 mm and the indenter was equipped with an instrumented hemispherical tip of diameter 10 mm. The impact speed was 4 ms⁻¹ and the incident impact energy was 30 J. Three tests were made for each specimen type. The impact strength, σ_{max} , was calculated from the IFWI load traces according to [8]

$$\sigma_{\max} = \frac{2.5 F_{\max}}{t^2} \quad (1)$$

where t is the thickness of the plate and F_{\max} is the maximum force.

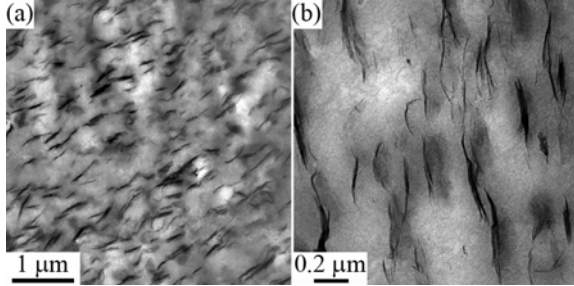


Fig. 1. TEM of thin sections from a PP-5.9 wt% MMT extruded film at two different magnifications.

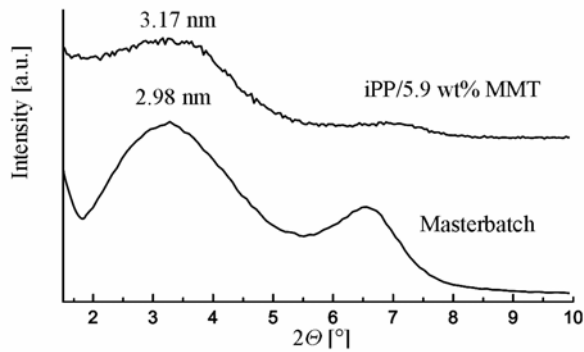


Fig. 2. WAXS patterns from the masterbatch and from PP-5.9 wt% MMT.

3 Results

3.1 PP-MMT nanocomposite morphology

The representative TEM image of a PP-5.9 wt% MMT film in Fig. 1 shows compounding to result in a homogeneous PP-MMT nanocomposite, even at relatively high MMT loadings. The morphology comprised a mixed intercalated-exfoliated structure dominated by intercalated MMT stacks with an aspect ratio of between 20 and 50, globally oriented along the extrusion direction. Dilution of the PP-5.9 wt% MMT base resin with PP also gave homogenous morphologies of this type, whereas direct melt compounding at relatively low MMT concentrations led to significant agglomeration of the MMT particles. WAXS patterns from compression molded sheets showed clear reflections corresponding to the regular

stacking of the individual MMT platelets consistent with the TEM observations, but also indicated an increase of about 6% (Fig. 2) in the interlayer spacing at all MMT concentrations after extrusion, an increase that was maintained in the extrusion-calendered films.

3.2 Rheological properties of the as-compounded PP-MMT

Fig. 3 shows the effect of MMT content on the viscosity, η , in steady state shear. The influence of the MMT was most marked at low shear rates, with an increase in η by almost one order of magnitude on addition of 2.4 wt% MMT, for example. At high effective shear rates, on the other hand, the PP matrix dominated the response. Thus, the broad Newtonian plateau observed for the pure PP was progressively reduced on MMT addition, and there was increasingly pronounced shear thinning, which may be attributed to break-down of a weak MMT network, and subsequent orientation and possibly deformation of the individual MMT domains during flow.

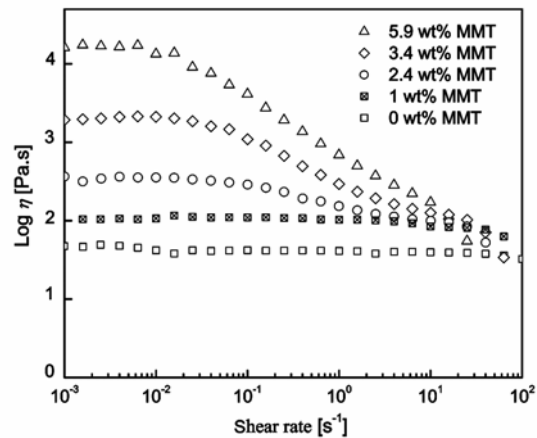


Fig. 3. The influence of MMT content on η in steady shear at 200 °C.

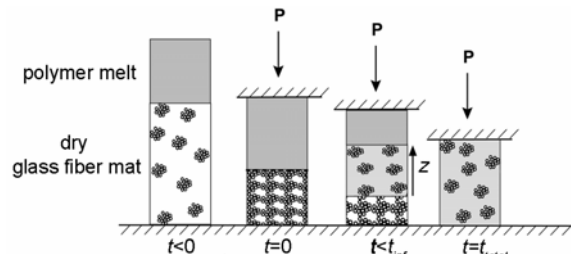


Fig. 4. Schematic of the impregnation process.

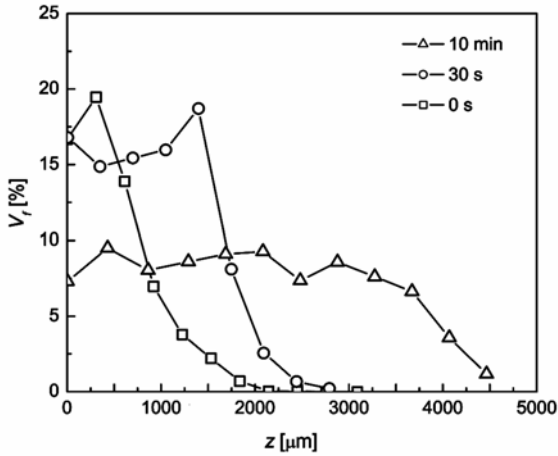


Fig. 5. Distribution in V_f at different stages of the impregnation process for a pure PP matrix.

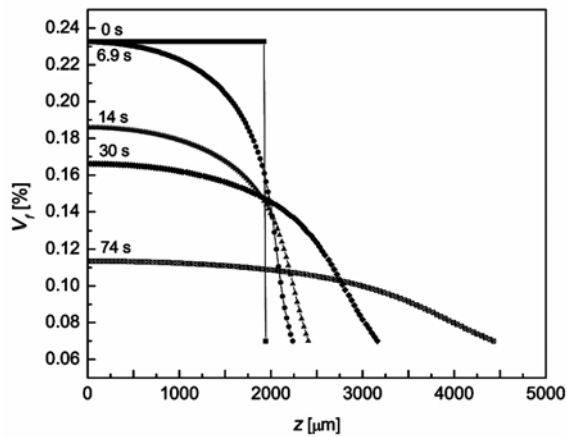


Fig. 6. Model predictions of the distribution in V_f at different stages of the impregnation process for a pure PP matrix.

3.3 Impregnation

Initial impregnation in the double blent press involves (i) compression of the GF mat ($t = 0$), (ii) infiltration of mat by the matrix ($t = t_{inf}$) and (iii) relaxation of the mat to give a homogeneous GF distribution, as sketched in Fig. 4 [6,7]. Experimental results for the distribution in the fiber volume fraction V_f at different stages of the impregnation process are shown for pure PP in Fig. 5, where the average value of V_f across the specimen width measured by optical microscopy has been plotted as a function of position, z , with respect to the infiltration front (see Fig. 4). In absence of applied pressure there was no infiltration due to gravity or capillary forces. Infiltration was therefore

assumed only to occur during and after mold closure. Indeed, in the case of the pure PP matrix, the glass fiber mat was fully wetted by the polymer melt immediately after closure of the mold and partial infiltration of the fiber bed could not be observed experimentally for $t > 0$. For short impregnation times, there was nevertheless a strong gradient in V_f throughout the specimen thickness, although this decreased with increasing t . Hence, for $t = 10$ min the glass fiber distribution was nearly homogeneous.

At an applied pressure of 0.2 MPa, the local shear rate in the polymer matrix does not exceed about 1 s^{-1} , and the Newtonian plateau extends to much higher shear rates for PP. Thus, the model of Michaud *et al.* [6] is applicable, assuming the infiltration to occur with a small local Reynolds number. In the present case, the permeability and stress-strain behavior of the fiber mats was found to be similar to that reported by Michaud *et al.* [9], V_f reaching 24 % as the applied pressure increased to 0.2 MPa, and the PP matrix viscosity was determined to be 64 Pa.s by shear rheometry. The predictions of the model are shown in Fig. 6. The agreement between these and the experimental data was reasonable given that factors such as friction at the mold walls were not taken into account in the calculations, the relatively small areas ($15 \times 4.5 \text{ mm}^2$) observed by optical microscopy compared with that of the representative volume element of the glass fiber mats (about 25 cm^2), and the uncertainties in the experimental impregnation times for short t . A measure of these uncertainties is the calculated infiltration time for the model preform of about 7 s. At much longer times (30 s), however, the experimental data correlated well with the calculated glass fiber distributions, particularly close to the bottom of the mold. Towards the top of the mold, the measured V_f were somewhat lower than the calculated values, which was attributed to an increase in experimental data scatter with decreasing glass fiber content. The model also predicted the glass mat to reach the top part of the mold after 74 s and that 160 s were sufficient to achieve complete relaxation of the glass mat, consistent with the experimental observations made after 10 min impregnation, for which the mean experimental value for V_f was about 8 %, i.e. only slightly higher than for the fully relaxed state (7 %). This discrepancy was ascribed to frictional effects, which prevent the mat from fully relaxing.

The local shear rate experienced by the PP-MMT nanocomposites during infiltration may again

be assumed not to exceed about 1 s^{-1} . This value corresponds to the Newtonian plateau for PP-1 wt% MMT, but for higher MMT concentrations the nanocomposites showed neither Newtonian, power-law nor Carreau-type behavior. Since existing impregnation models are not capable of providing a realistic description even for relatively simple non-linear flow laws, for the purpose of estimating the effect of the MMT, Newtonian behavior was assumed and the viscosity taken to be that observed at a shear rate of 1 s^{-1} for the composition in question. Thus, the effective viscosities of PP-3.4 wt% MMT and PP-5.9 wt% MMT used in the calculations were 294 and 692 Pa.s respectively. The estimated infiltration times, the times for the mat to reach the upper part of the mold and the times for the mat to relax fully are given in Fig. 7. The use of a linear flow law resulted in direct proportionality between the calculated times and the matrix viscosity, facilitating extrapolation to other compositions.

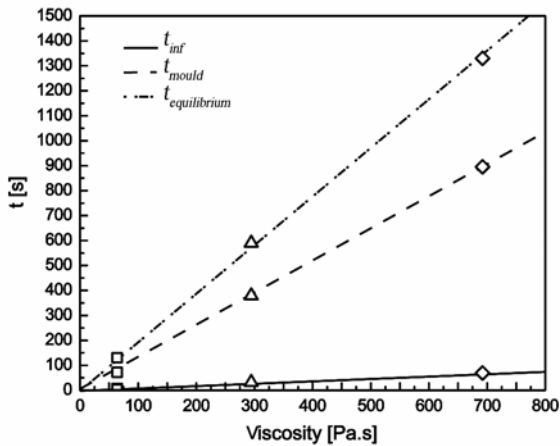


Fig. 7. Infiltration time, t_{inf} , time for the glass mat to reach the end of the mold, t_{mould} , and time for the glass mat to relax fully, $t_{equilibrium}$, as a function of the polymer matrix viscosity ((□) 0wt% MMT, (Δ) 3.4wt% MMT, (◇) 5.9 wt% MMT), for impregnation under an applied pressure of 0.2 MPa.

It was confirmed experimentally that infiltration times were longer for the high viscosity matrices, so that for PP-5.9 wt%, infiltration remained incomplete after 30 s (cf. the predicted value of t_{inf} of about 70 s in Fig. 7). It was therefore possible to observe the different stages of infiltration as shown in Fig. 8. In Fig. 8(a), where infiltration is incomplete, the glass fibers are compacted in the lower part of the specimen. In Fig. 8(b), infiltration

is again incomplete but the glass mat has undergone significant relaxation. Finally, in Fig. 8(c), infiltration is complete and the glass fiber distribution is relatively homogeneous (cf. the predicted value of $t_{equilibrium}$ of about 1300 s in Fig. 7).

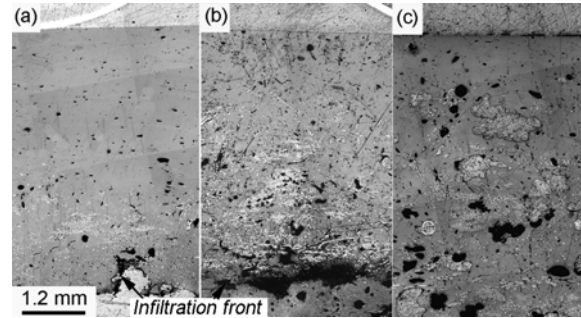


Fig. 8. Optical micrographs from a preform with a PP-5.9 wt% MMT matrix for different t : (a) 0 s, (b) 30 s, and (c) 10 min, showing infiltration of the fiber mat and relaxation of the mat into the nanocomposite matrix.

In order to facilitate further comparison, the experimental results for the glass fiber distributions in the different specimens have been represented as follows. z is normalized with respect to the thickness of the part of specimen containing the polymer matrix and the impregnated glass fibers, z_0 . V_f is then determined in successive transverse segments of the specimen and normalized with respect to the overall glass fiber volume fraction. Finally, the sum of the V_f for all the segments up to and including that at position z is plotted as a function of $z' = z/z_0$. Thus, the data for the pure PP matrix in Fig. 5 convert to those in Fig. 9(a). The reference line $x = y$ corresponds to an ideal specimen in which the glass fiber distribution is homogeneous. The advantage of this representation is that the glass fiber distributions in specimens with different impregnation kinetics may be compared directly.

The data in Fig. 9(a) for the pure PP matrix were relatively close to the reference line for all t . For the PP-5.9 wt% matrix, on the other hand (Fig. 9(b)), the relaxation of the glass fiber mat was much slower and the homogeneity of the fiber distribution changed significantly with t . Thus after 0 s and 30 s of impregnation, substantial gradients in V_f persisted in the specimen. However, for $t = 10 \text{ min}$ the glass fiber distribution was similar to that observed for pure PP. Fig. 10(a) compares the glass fiber distribution for 0 wt%, 3.4 wt% and 5.9 wt% MMT immediately after closure of the mold, further

illustrating the trend towards increased gradients in V_f as the MMT content increased at a given t .

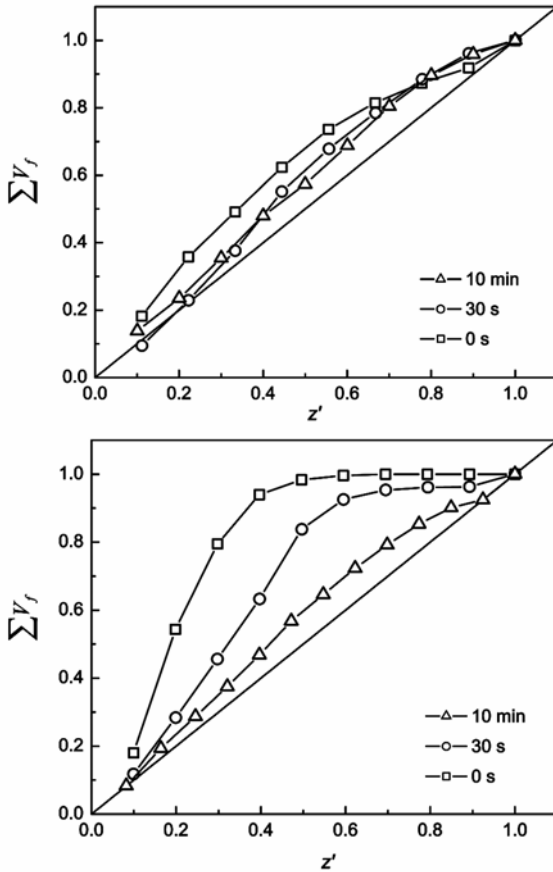


Fig. 9. Cumulative relative fiber volume fractions at different t for (a) a pure PP matrix and (b) a PP-5.9 wt% MMT matrix.

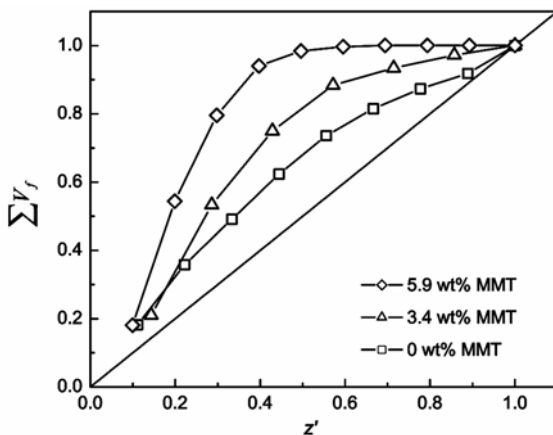


Fig. 10. Cumulative relative fiber volume fractions at $t = 0$ for different matrix MMT contents.

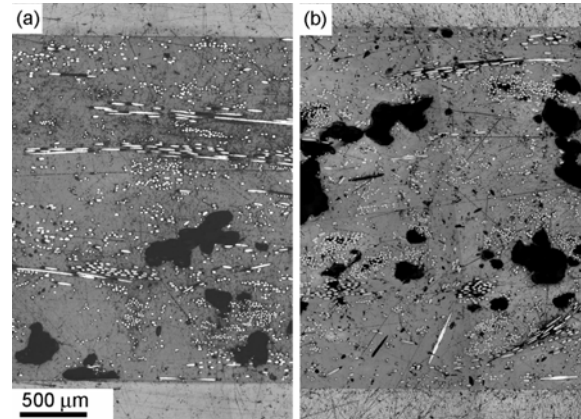


Fig. 11. Optical micrographs from the GMT-like specimens for $t = 30$ s with (a) a pure PP matrix and (b) a PP-5.9 wt% MMT matrix.

Representative optical micrographs of industrial GMT-like specimens impregnated with PP-0 wt% MMT and PP-5.9 wt% MMT matrices are shown in Figs. 11(a) and (b) for $t = 30$ s. A homogeneous glass fiber distribution is apparent in each case. Thus, for the significantly shorter impregnation distances associated with the interleaved preforms, the increased matrix viscosity of the nanocomposite matrices did not appear to be critical for the glass fiber distribution, even for relatively short t . The full cross sections corresponding to Fig. 11 are shown in Fig. 12. The dark areas are regions of closed porosity and the light gray areas are regions of open porosity (filled with the embedding resin). The porosity of the GMT-like specimens generally decreased slightly with increasing MMT content but remained between 11 and 18 vol %, which compares with values of about 14 vol% characteristic of industrial GMT blanks [4].

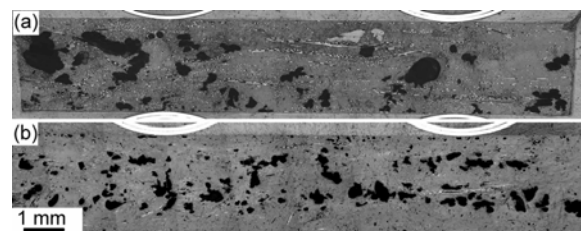


Fig. 12. Optical micrographs from the GMT-like specimens showing the porosity after 30 s of impregnation for (a) a pure PP, and (b) a PP-5.9 wt% MMT matrix.

3.4 Mechanical properties

Addition of MMT to PP films resulted in a significant increase in Young's modulus, E , in the extrusion direction, reaching nominally twice the value for pure PP at 5.9 wt% MMT. However, the differences were smaller in the transverse direction, reflecting the orientation of the MMT platelets along the extrusion direction observed by TEM (Fig. 1). This anisotropy was also apparent in the crack initiation resistance of the films, measured using a modified essential work of fracture (EWF) analysis of double edge-notched tensile specimens, described in more detail elsewhere [10]. The crack resistance increased at intermediate MMT contents for cracks initiating perpendicular to the orientation direction, but decreased for cracks initiating parallel to it. This may be rationalized in terms of limited adhesion between the PP and the MMT and cohesive failure of (unexfoliated) MMT particles parallel or nearly parallel to the crack propagation direction [10].

The 3-point bend tests on the consolidated composites confirmed previous observations [3] of significant improvements in flexural modulus and strength over a range of temperatures. Data for the flexural modulus and strength are given in Fig. 13 and Fig. 14. In order to assess the role of the MMT in the observed improvement in stiffness, a theoretical estimate of the composite modulus, E_c , has been derived from the matrix mechanical property data using the Cox-Krenchel equation [11]:

$$E_c = \eta_0 \eta_l V_f E_f + (1 - V_f) E_m \quad (2)$$

where η_l is a fiber length efficiency factor that depends on the aspect ratio of the fibers, η_0 depends on the fiber orientation and E_m and E_f are the matrix and fiber moduli respectively.

In GMT materials, $\eta_l = 1$, for E-glass, $E_f = 76$ GPa [12] and E_m was taken from tensile test data for injection moldings. The theoretical bounds on E_c corresponding to a random in-plane alignment of the fibers ($\eta_0 = 0.375$), generally assumed for GMT materials, and a random 3D alignment ($\eta_0 = 0.2$) are shown in Fig. 13. The observed modulus for the pure PP matrix based GMT was close to the lower theoretical bound for E_c . However, the model increasingly underestimated the stiffness as the MMT content increased, suggesting addition of MMT (and the associated compatibilizers) to act in synergy with the fiber reinforcement. At higher temperatures, however, this effect was reduced, and the data for 90 °C showed little deviation from the model, i.e. relatively little influence of the MMT on

the global stiffness. Zhao *et al.* [13] have reported comparable room temperature stiffness and strength increases in GMT specimens (12.5 vol% GF) containing mica.

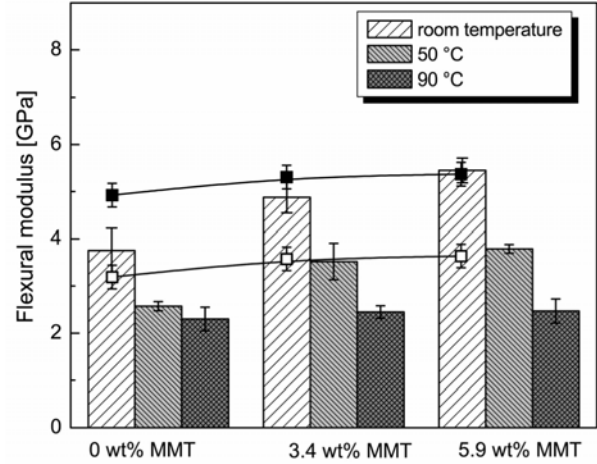


Fig. 13. Flexural modulus of GMT specimens as a function of MMT concentration at different temperatures. The squares correspond to estimates from equation (2) for $\eta_0 = 0.375$ (lower curve) and $\eta_0 = 0.2$ (upper curve).

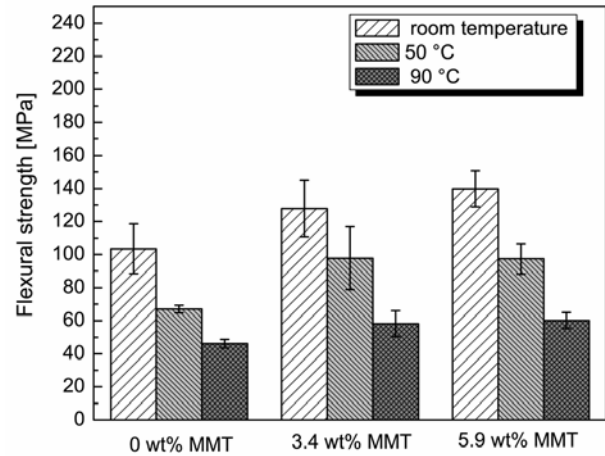


Fig. 14. Flexural strength of GMT specimens as a function of MMT concentration at different temperatures.

The room temperature impact strengths from FWI tests (Fig. 15) decreased with MMT content, with an approximately 40% reduction being observed for PP-5.9 wt% MMT with respect to the pure PP matrix. Inspection of the damaged samples showed the perforation area to be similar at all MMT concentrations and test temperatures, i.e. a

circumferential crack with a perforation size close to that of the dart. This indicated the fracture mode to be relatively ductile (absence of radial cracking), with efficient stress transfer within the mat. The impact strength decreased at 90 °C for the pure matrix, presumably owing to increased matrix ductility but, as with the stiffness and the strength, the effect of MMT concentration on σ_{max} appeared less marked at 90 °C than at room temperature, so that the temperature had relatively little overall influence. However, the impact energy, which also decreased monotonically with MMT content at room temperature, showed a pronounced maximum at 90 °C at about 3 wt% MMT, reaching more than twice the value measured for the pure matrix at the same temperature.

To investigate the mechanisms underlying this behavior, SEM micrographs were taken from the fracture surfaces of the various composites. Fig. 17 shows typical images from the room temperature fracture surfaces of pure PP-based GMT (Fig. 17(a)) and PP-5.9 wt% MMT-based GMT (Fig. 17(b)). For the pure PP, the matrix regions were relatively smooth and featureless, indicating brittle fracture. However, significant debonding of the glass fibers was also visible, with a very clean glass surface, characteristic of poor interfacial adhesion. The matrix was significantly rougher for the PP-5.9 wt% MMT matrix, possibly reflecting crack deviation by the MMT particles, as inferred for the precursor films. Furthermore, matrix residues were visible at the surface of glass fibers indicating better interfacial adhesion. At 90 °C, significant fiber pull-out was again observed with the pure PP, but also a relatively rough matrix fracture surface, consistent with a transition to a more ductile matrix failure mode. On the other hand, the fracture surfaces for the PP-5.9 wt% MMT-based GMT tested at 90 °C were very similar to those obtained for the specimens tested at room temperature. It is inferred that the MMT particles may act as matrix tougheners in this system, and hence increase the impact energy, but that the effect is most marked at elevated temperatures, at which the matrix is relatively ductile.

4 Conclusions

It has been shown that MMT concentrations of up to 5.9 wt% in PP precursor films are compatible with conventional GMT processing. The corresponding composites showed significant increases in flexural strength and stiffness, and

although impact strengths were somewhat reduced, the high temperature impact energy passed through a maximum at about 3 wt% MMT content. These results are considered encouraging, and the next step in this work will be to undertake scale-up trials comprising tests on a comprehensive range of properties and costing for potential applications.

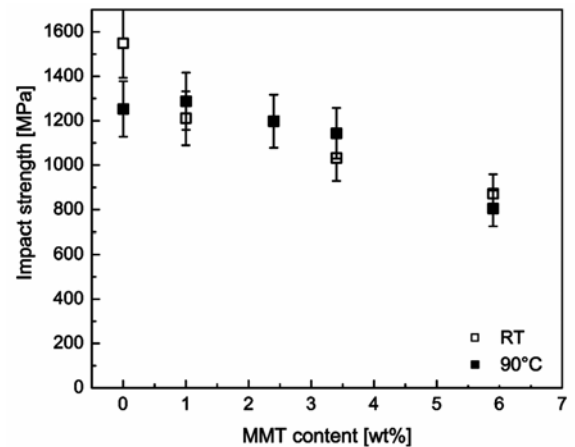


Fig. 15. Impact strength versus MMT content for PP-MMT-based GMT impacted at room temperature and 90 °C.

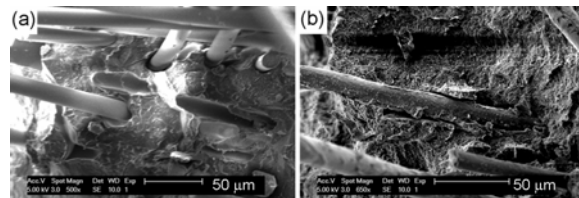


Fig. 16. SEM micrographs of impact fracture surface of (a) PP and (b) PP-5.9 wt% MMT-based GMT, impacted at room temperature.

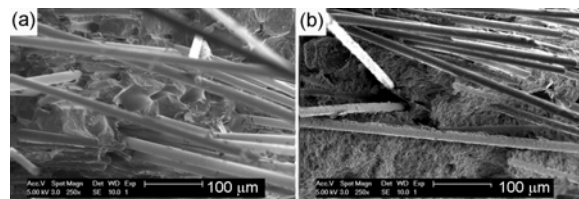


Fig. 17. SEM micrographs of impact fracture surface of (a) PP and (b) PP-5.9 wt% MMT-based GMT, impacted at 90 °C.

Acknowledgment

The authors would like to thank the Centre Interdépartemental de Microscopie Electronique

(CIME) of the EPFL for their support during this work

References

- [1] Roy, S., Hussain, F., Vengadassalam, K. and Lu, H. "Manufacturing, Mechanical Characterization, and Modeling of a Pultruded Thermoplastic Nanocomposite", in *"Nanoengineering of Structural, Functional, and Smart Materials"*, Schulz, M.J., Kelker, A.D. and Sunderasen, M.J. (eds.), 1st edition, CRC Taylor & Francis, USA, Ch. 17, 2006.
- [2] Solomon M.J., Almusallam A.S., Seefeldt K.F., Somwangthanaroj A. and Varadan P. "Rheology of polypropylene/clay hybrid materials". *Macromolecules*, Vol. 34, No. 6, pp 1864-1872, 2001.
- [3] Houphouët-Boigny, C., Plummer, C.J.G. Wakeman, M.D., Manson, J.-A.E. "Hybrid glass-fiber reinforced thermoplastic nanocomposites", *26th International SAMPE Europe conference*, Paris, France, April 2005.
- [4] Wakeman, M.D., Cain, T.A., Rudd, C.D. and Long, A.C. "Compression Moulding of Glass and Polypropylene Composites for Optimised Macro- and Micro-Mechanical Properties II. Glass-Mat-Reinforced Thermoplastics", *Comp. Sci. & Tech.*, Vol. 59, pp 709-726, 1999.
- [5] Ford, R.A. "Semi-finished thermoplastic composites-realising their potential", *Mater. & Design*, Vol. 25, pp 631-636, 2004.
- [6] Michaud V. and Manson J.-A.-E. "Impregnation of compressible fiber mats with a thermoplastic resin. Part I: Theory". *J. Comp. Mater.*, Vol. 35, No. 13, pp 1150-1173, 2001.
- [7] Jespersen, S.T., Wakeman, M.D., Cramer, D., Michaud V. and Manson, J.-A.E., "Film stacking impregnation model for thermoplastic composites applied to a novel netshape preforming process", *FPCM8 – International Conference on Flow Processes in Composite Materials*, 2006
- [8] Czigany, T. and Karger-Kocsis, J. "Comparison of the instrumented falling weight impact response of polypropylene composites reinforced by continuous and discontinuous fiber mats", *J. Reinforced Plastics & Comp.*, Vol. 20, pp 996-1012, 2001.
- [9] Michaud, V., Tornqvist, R. and Manson J.-A.-E. "Impregnation of compressible fiber mats with a thermoplastic resin. Part II: Experiments", *J. Comp. Mater.*, Vol. 35, pp 1174-1200, 2001.
- [10] Houphouët-Boigny, C., Plummer, C.J.G. Wakeman, M.D., Manson, J.-A.E. "Hybrid glass-fiber reinforced thermoplastic nanocomposites", *to be submitted*.
- [11] Thomason, J.L. "The influence of fibre length and concentration on the properties of glass fibre reinforced polypropylene. 6. The properties of injection moulded long fibre PP at high fibre content", *Comp. Part A - Appl. Sci. & Manufacturing*, Vol. 36, pp 995-1003, 2005.
- [12] Lubin, G. *"Handbook of composites"*, Van Nostrand Reinhold, New York, 1982.
- [13] Zhao, R.F., Zhou X.D. and Dai, G. "Effect of the microstructure of GMT on its mechanical properties", *Polym. Comp.*, Vol. 23, pp 1026-1035, 2002.